# Support vector machine classification and characterization of age-related reorganization of functional brain networks

**Timothy B. Meier**[1], **Alok S. Desphande**[2], **Svyatoslav Vergun**[3], **Veena A. Nair**[4], **Jie Song**[5], **Bharat B. Biswal**[6], **Mary E. Meyerand**[3,5], **Rasmus M. Birn**[7], and **Vivek Prabhakaran**[1,4]

[1]Neuroscience Training Program, University of Wisconsin-Madison, Madison, WI 53705, USA

[2]Department of Elec. and Comp. Engineering, University of Wisconsin-Madison, Madison, WI 53706, USA

[3]Department of Medical Physics, University of Wisconsin-Madison, Madison, WI 53705, USA

[4]Department of Radiology, University of Wisconsin-Madison, Madison, WI 53792, USA

[5]Department of Biomedical Engineering, University of Wisconsin-Madison, Madison, WI 53706, USA

[6]Department of Radiology, University of Medicine and Dentistry of New Jersey, Newark, NJ 07103, USA

[7]Department of Psychiatry, University of Wisconsin-Madison, Madison, WI 53719, USA

## Abstract

Most of what is known about the reorganization of functional brain networks that accompanies normal aging is based on neuroimaging studies in which participants perform specific tasks. In these studies, reorganization is defined by the differences in task activation between young and old adults. However, task activation differences could be the result of differences in task performance, strategy, or motivation, and not necessarily reflect reorganization. Resting-state fMRI provides a method of investigating functional brain networks without such confounds. Here, a support vector machine (SVM) classifier was used in an attempt to differentiate older adults from younger adults based on their resting-state functional connectivity. In addition, the information used by the SVM was investigated to see what functional connections best differentiated younger adult brains from older adult brains. Three separate resting-state scans from 26 younger adults (18-35 yrs) and 26 older adults (55-85) were obtained from the International Consortium for Brain Mapping (ICBM) dataset made publically available in the 1000 Functional Connectomes project www.nitrc.org/projects/fcon_1000. 100 seed-regions from four functional networks with 5 mm$^3$ radius were defined based on a recent study using machine learning classifiers on adolescent brains. Time-series for every seed-region were averaged and three matrices of z-transformed correlation coefficients were created for each subject corresponding to each individual's three resting-state scans. SVM was then applied using leave-one-out cross-validation. The SVM classifier was 84% accurate in classifying older and younger adult brains. The majority of the connections used by the classifier to distinguish subjects by age came from seed-regions belonging

Address Correspondence to: Timothy B. Meier, University of Wisconsin-Madison, Neuroscience Training Program, 1310d Wisconsin Institutes for Medical Research, 1111 Highland Ave., Madison, WI 53705, Phone: 608-232-3343, Fax: 608-265-4152, tbmeier@wisc.edu.

to the sensorimotor and cingulo-opercular networks. These results suggest that age-related decreases in positive correlations within the cingulo-opercular and default networks, and decreases in negative correlations between the default and sensorimotor networks, are the distinguishing characteristics of age-related reorganization.

## Keywords

machine learning; resting-state fMRI; aging; reorganization

## 1. Introduction

Until relatively recently, most of our knowledge regarding the age-related reorganization of functional networks in the human brain has been based on neuroimaging studies comparing differences in task activity between younger and older adults. However, following an explosion of research into resting-state functional connectivity, it has been proposed that all functional networks that are utilized for task performance are present during rest in the form of correlations between low frequency fluctuations (Biswal et al., 1995; Smith et al., 2009). Resting-state fMRI allows the investigation of age-related changes in functional networks without confounds of task studies, such as performance, motivation, and the use of divergent strategies.

Relatively few studies have attempted to characterize age-related reorganization of functional networks at the brain-wide level using resting-state functional connectivity (Biswal et al., 2010). In one such study, Meunier et al. completed a graph theoretical analysis on resting-state data investigating the effects of aging on the modular organization of functional networks (2009). They found that large modules, or networks, observed in young healthy adults were split up into smaller modules in older adults. In addition, they observed a shift in the hubs of modular connectivity, where the hubs for older adults were located in more posterior regions compared to younger adults (Meunier et al., 2009). A separate study investigating global functional connectivity differences in homotopic regions of the brain between younger and older adults found that functional connectivity between homotopic areas decreases from adolescence to adulthood, and then increases again with advancing age in adulthood (Zuo et al., 2010). However, several questions regarding the exact nature of the changes in brain networks that accompany age remain.

One powerful method available to investigate the age-related reorganization of functional networks is the use of machine learning classifiers (Pereira et al., 2009). Machine learning classifiers, such as support vector machines (SVM), entail selecting independent variables, known as features, and using these features to predict the class membership of an individual example. The features are assigned parameters, called weights, by applying the SVM algorithm to a training dataset with known class labels. In essence, the feature weight corresponds to the relative contribution of a specific feature to the classifier's ability to successfully differentiate the two groups. After feature weights are calculated, the classifier can then be applied to a separate dataset, known as the testing dataset, and the performance of the classifier can be assessed in terms of its accuracy in classifying examples to the correct class.

The use of SVM on resting-state fMRI data has several advantages over traditional univariate methods. For example, the robustness of findings on group differences can be measured in terms of the accuracy in which these findings classify individual subjects. Importantly, SVM allows the identification of features that contributed the most to subject classification, providing insight into the defining differences between two groups.

Machine learning classifiers, including SVM, have been successfully applied to resting-state fMRI data in the classification of major depressive disorder, schizophrenia, and adolescent brains from normal adult brains (Craddock et al., 2009; Shen et al., 2010; Supekar et al., 2009). A recent study by Dosenbach and colleagues used SVM (and a related method support vector regression) to classify adolescent and adult brains based on resting-state functional connectivity (2010). They observed that the distinguishing characteristic for successful classification between child and adult brains was a decrease in correlations among short-range connections, along with an increase in correlations among long-range connections with increasing age.

In this study, a commonly used machine learning method namely the SVM was used to discriminate healthy younger and older adults based on their resting-state functional connectivity. We hypothesized that older and younger adult brains could be successfully classified based on their resting-state functional connectivity with the use of binary SVM. In addition, the major goal of this study was to use the information provided by SVM to identify what features (in our case functional connections) contributed the most to the success of the classifier. It is our hope that by thoroughly investigating these features we can identify patterns of network and seed-region differences that represent the distinguishing functional network changes that occur with normal aging.

## 2. Materials and Methods

Resting-state data from 26 right-handed younger adults (18-35 yrs, mean = 24.7 yrs ± 0.9 SEM, 12 male, 14 females) and 26 right-handed older adults (55-85 yrs, mean = 64.7 yrs ± 1.56 SEM, 11 male, 15 female) were obtained from the International Consortium for Brain Mapping (ICBM) dataset made publically available in the 1000 Functional Connectomes project www.nitrc.org/projects/fcon_1000 (Biswal et al., 2010). This dataset includes three separate resting-state scans for each subject in which 23 axial slices were acquired on a 3T scanner and comprised of 128 time points using a gradient-echo EPI sequence with TR = 2 seconds where subjects lied in the scanner with their eyes closed. Out of 78 total scans in older adults, 42 were acquired with spatial resolution of $4 \times 4 \times 5.5$ mm, while 36 were acquired with spatial resolution of $4 \times 4 \times 4$ mm. Out of the 78 total scans in younger adults, 36 were acquired with spatial resolution of $4 \times 4 \times 5.5$ mm, while 42 were acquired with spatial resolution of $4 \times 4 \times 4$ mm. Information regarding this dataset is available at www.nitrc.org.

### 2.1. Preprocessing

Functional data were preprocessed using slightly modified scripts included in the 1000 Functional Connectomes Project using a combination of FSL and AFNI (Biswal et al., 2010; Cox, 1996; Smith et al., 2004; Woolrich et al., 2009). All images were first deobliqued and reoriented to RPI orientation for use in FSL. EPIs were motion and slice-time corrected, spatially smoothed using a Gaussian kernel of 6 mm FWHM, and scaled to the grand mean. Time series were then band-pass filtered (0.005 – 0.1 Hz) and linear and quadratic trends were removed. The eighth image of each scan was used to register the EPI scan to the high resolution anatomical scan that was acquired during the same session of the particular EPI.

In order to control for participant movement and physiological processes, motion parameters, global signal, white matter signal, and CSF signal were regressed from the time series. The global signal was calculated by averaging across all voxels in the brain. White matter and CSF masks were created by the segmentation of each individual's structural image using FSL's FAST program and then applied to each EPI to extract the white matter and CSF signals. Following the removal of these nuisance variables, the residual time series

for each scan were demeaned, re-sampled to 3 mm$^3$, and registered to MNI152 standard space using FSL's FLIRT program.

## 2.2. Seed-based connectivity

Time courses were extracted from predefined regions of interest derived from a series of meta-analyses of task-related fMRI studies, as described in Dosenbach et al. (2010). In their study, Dosenbach and colleagues investigated 160 total seed-regions from six different networks. We focused on seed-regions located in the default network, sensorimotor network, fronto-parietal network, and the cingulo-opercular network. Figure 1 displays the seed-regions used. In order to calculate seed-regions that were common among all subjects, an inclusive mask of the spatially normalized residuals was created and applied to every EPI. This insured that seed-regions in which some or all participants had no signal or EPI brain coverage were not included in our analysis.

The time series from 100 five mm$^3$ radius spherical seed-regions that survived the inclusive mask were extracted from the spatially standardized residuals for every EPI scan. The resulting time series for each seed-region from each of the three EPI scans per subject were then imported into Matlab (Mathworks) and correlated against every other seed-region, resulting in the creation of three $100 \times 100$ matrices of correlation coefficients for each individual. Correlation coefficients were z-transformed using Fisher's r-to-z transformation to normalize the distribution.

## 2.3. Binary SVM classification and leave-one-out cross-validation

Soft-margin SVM classification (with regularization parameter C = 0.5) was performed using the Spider Machine Learning Toolbox (Weston et al., 2005) implemented in Matlab (Mathworks). A radial basis function was used as the underlying kernel to map the data in higher-dimension vector space and apply a linear decision function to classify individual scans as being from either the younger or older adult group. Leave-one-out cross-validation (LOOCV) was used for tuning the SVM hyper-parameters and estimating the classifier's accuracy. The benefit of LOOCV is that the same dataset can be used for both the training and testing of the classifier (Pereira et al., 2009). For each round of LOOCV, a subject's data was removed (all three scans to avoid twinning bias) and the top 200 features (connections) were selected using two-sample t-tests (not assuming equal variance) on the training set and ranked according to their absolute t-statistics in descending order. The criterion of retaining top 200 features was based upon the fact that approximately the same number of features survived the same t-test on the whole data after False Discovery Rate correction. The classifier was then trained, and feature weights were estimated on the remaining subjects' datasets (serving as the training dataset). The three scans of the subject that were left out of the training set served as the testing dataset, and were each separately classified as being either young or old. This process was repeated for every subject and the total accuracy of the classifier was determined by the percent of scans which were correctly categorized.

# 3. Results

## 3.1. Overall classifier performance

The classifier successfully discriminated older adults from younger adults at an accuracy of 84%. Given the equal number of older and younger adults in our sample, chance performance of the classifier would have yielded an accuracy of 50% (the null hypothesis). Therefore, we treated each fold of the leave one out cross validation as a Bernoulli trial with success probability of 0.5, as specified by Pereira et al. (2009). By comparing the number of true positives to the total number of examples (scans to be classified as young or old) we

observed the probability of our measured accuracy occurring by chance. The 84% accuracy of the classifier was highly significant, having a p value < 0.0000001.

## 3.2. Consensus features

Two-hundred features, defined as the functional connectivity between two seed-regions, were obtained from each round of LOOCV. From these, 126 features, known as consensus features, were found to be common across every round. Table 1 lists the consensus features with negative predictor weights corresponding to seed-region pairs in which older adults had significantly higher correlation coefficients than younger adults. Table 2 lists consensus features with positive predictor weights corresponding to seed-region pairs in which younger adults had significantly higher correlation coefficients than older adults.

The goal of the present study was to identify the functional connections that distinguish older adult brains from younger adult brains. To identify brain regions that undergo significant age-related changes in functional connectivity, the contribution of each seed-region to the overall ability of the classifier to accurately discriminate between age groups can be assessed by summing one-half of the feature weights associated with that seed-region. For this study, we used a non-linear radial basis function as the kernel for the SVM classification, to be consistent with the study by Dosenbach and colleagues (2010). The use of a non-linear kernel limits the interpretation of the SVM weights in high dimensional feature space, and also prevents the exact transformation of feature weights from feature space back to input space (Scholkopf et al., 1999). Therefore, we find an approximation of feature weight by performing a two sample t-test between the young and old age groups for each connection (feature) and use the resulting t-score as our feature weight.

The single seed-region with the greatest amount of feature weight associated with it was a seed-region located in the left precuneus, near the border of the cingulate (MNI coordinates -3 -38 45). Table 3 displays the top ten seed-regions when ranked by total feature weight. The seed-region that contributed to the second-most feature weights was located in the right post-central gyrus (MNI coordinates 46 -20 45). The third and fourth largest contributions came from the right pre-SMA (MNI coordinates 0 5 51) and SMA (0 -1 52), respectively.

The z-transformed correlation coefficients from the consensus features for both the younger and older adult groups were analyzed to determine the exact nature of the functional connectivity changes that contributed to the total feature weight used in the SVM classification (Tables 1 and 2). Of the total feature weight entered into the SVM, 37% came from pairs of seed-regions that displayed a decrease in correlation coefficients with age, where older adults displayed a significantly lower correlation between seed-region pairs than younger adults (Figure 2a). Positive correlations that were significantly higher in older adults than younger adults accounted for 31% of the total feature weight. Negative correlations that were significantly less negative in older adults than younger adults contributed to 32% of the total feature weight. Figure 3 is an illustration of the consensus features connected to their associated see-regions. Although in terms of SVM performance decreases in negative correlations and increases in positive correlations with age were equivalent (i.e., both resulted in negative weights), we differentiated the patterns in this nature because of the hypothesized physiological significance of a positive correlation and a negative correlation (anti-correlation) between two regions (Fox et al., 2005).

The seed-regions used in this study have been previously classified as belonging to four different functional networks by Dosenbach et al. (2010). Seed-regions from the fronto-parietal, cingulo-opercular, sensorimotor, and default network were investigated here. In order to identify what functional networks display the greatest amount of age-related change, the contribution of each network to the SVM classification was compared by

summing the weight from all of the seed-regions classified as belonging to a certain network. As seen in Figure 2b, seeds from the sensorimotor network contributed the highest percentage of the feature weight, although all four networks contributed. We were able to further characterize each seed-region pair as either being between two different networks or being within a single network. Based on our SVM results, the majority of seed-region pairs that were significantly more connected in older adults (or less negatively correlated) were between network connections. Conversely, the majority of seed-region pairs that were significantly less connected in older adults were approximately half within network connections and half between network connections.

To get an in depth understanding of what types of age-related changes each network underwent, the contribution of each individual network to each of the above-mentioned scenarios was calculated.

### 3.3. Increased positive correlations with age

**3.3.1. Between networks—**Sixty-three percent of the weight from seed-region pairs that had an increase positive correlation with age were from connections between two different networks (Figure 4a). Of these, the majority (57%) of the weight came from connections between seed-regions in the sensorimotor and cingulo-opercular networks, 16% was between seed-regions in the sensorimotor and fronto-parietal networks, 14% was between seed-regions in the default and the fronto-parietal networks, 10% was between seed-regions in the fronto-parietal and cingulo-opercular, and 3% was between seed-regions in the cingulo-opercular and default networks.

**3.3.2. Within networks—**Thirty-seven percent of the weight coming from connections that were more positively correlated in older adults than younger adults was from within network connections. Of these, sensorimotor made up 79%, default made up 14%, and fronto-parietal made up 7%.

### 3.4. Decreased negative correlations with age

**3.4.1. Between networks—**All of the seed-region pairs that were significantly less negatively connected in older adults than in younger adults were between networks (Figure 4b). The majority of the feature weight from these seed-regions (70%) was between the seed-regions in the sensorimotor and default networks. Connections between the cingulo-opercular network and the default network accounted for 20% of the feature weight, while connections between the fronto-parietal and sensorimotor networks contributed 7% of the weight, and the cingulo-opercular and the fronto-parietal networks contributed 3% of the weight.

### 3.5. Decreased positive correlations with age

**3.5.1. Between networks—**Just over half (51%) of the weight from seed-region correlations that became less positive with age was from between network connections (Figure 4c). Of these, 73% were between the sensorimotor and cingulo-opercular networks, 15% were between the fronto-parietal and cingulo-opercular networks, 8% were between the fronto-parietal and sensorimotor networks, and 4% were between the default and sensorimotor networks.

**3.5.2. Within networks—**Within network connections contributed 49% of the weight coming from connections that were less positively correlated in older adults than younger adults. Of the within network connections 49% of the weight came from the cingulo-opercular network, 30% came from the sensorimotor network, 17% came from the default network, and 4% came from the fronto-parietal network.

### 3.6. Analysis by network

The feature weights belonging to each individual network was also classified by what type of connections they were and by what other networks they were connected to in order to understand the exact nature of the changes each network underwent.

**3.6.1. Fronto-parietal—**The connections accounting for the weight involving the fronto-parietal network were analyzed. Eighty-three percent of all of the weight coming from connections that included a fronto-parietal seed-region was from between network connections, whereas within network connections accounted for 17% (Figure 5a). Of the fronto-parietal connections that were between networks, 50% of the feature weight came from connections that increased positive correlation with age, 29% came from decreased positive correlation with age, and 21% came from connections that decreased positive correlation with age. Of the fronto-parietal connections that were within network, 52% increased positive correlation with age and 48% decreased positive correlation with age.

**3.6.2. Cingulo-opercular—**From the features that included the cingulo-opercular network, 68% of the weight was from between network connections while 32% was from connections within the cingulo-opercular network (Figure 5b). Forty-four percent of the weight coming from between network connections decreased positive correlation with age, while 36% increased positive correlation with age and 20% decreased negative correlation with age. Of the weight coming from connections that were within the cingulo-opercular network, 100% decreased positive correlation with age.

**3.6.3. Sensorimotor—**Sixty-five percent of the weight coming from features that included the sensorimotor network was between network connections and 35% was within network connections (Figure 5c). Among the weight coming from between network connections that included the sensorimotor network, 45% decreased negative correlation with age, 26% increased positive correlation with age, and 29% decreased positive correlation with age. Among the weight derived from within sensorimotor connections, 63% increased positive correlation with age and 37% decreased positive correlation with age.

**3.6.4. Default—**The feature weight attributed to connections involving the default network were 78% between network connections and 22% within network connections (Figure 5d). Of the weight coming from between network connections that included the default network, 88% was from connections that decreased in negative correlation with age, 10% was from connections that increased in positive correlation with age, and 2% was from connections that decreased in positive correlation with age. Of the weight that came from within default network connections, 65% decreased positive correlation with age, 35% increased positive correlation with age.

### 3.7. Seed-to-seed distance

Consensus features were also characterized by the Euclidian distance between the seed-to-seed connections to determine if there were any patterns in the age-related functional connectivity differences. Connections were grouped according to the differences in correlation coefficients in the three general scenarios described above and the distances were compared using two sample t-tests with unequal variance (Figure 6). Connections that were significantly more positively correlated in older adults than younger adults ($42.27 \pm 3.87$ mm SEM, n = 38) were significantly shorter than both connections that were less negatively correlated in older adults ($56.33 \pm 3.16$ mm SEM, n = 40; t(76) = -2.826, p < 0.01), and connections that were less positively correlated in older adults ($57.13 \pm 2.95$ mm SEM, n = 48; t(84) = -3.112, p < 0.005). There was no difference between connections that were less

negatively correlated in older adults and connections that were less positively correlated with age.

## 4. Discussion

The goal of the current study was to identify the distinguishing age-related differences in resting state functional connectivity. The feature weights derived from SVM classification provide a means of doing so as the success of the SVM classification is dependent on the weights assigned to each feature. The contribution of individual seed-regions and networks to the success of the SVM can be assessed by summing the feature weight associated with each.

Based on our analysis of the feature weights, every single network as previously defined by Dosenbach et al. (2010) that we investigated made a large contribution to the SVM classification (Figure 2b). Interestingly, the greatest contribution came from seed-regions located in the sensorimotor network. This is reflected by the fact that five of the top ten seed-regions that contributed the most feature weight belonged to this network (Table 3). Although not as extensively studied as age-related changes in cognition, numerous studies have established that normal aging is accompanied by a general decline in simple sensorimotor function associated with varying levels of task-related increases in brain activation and functional connectivity (Calautti et al., 2001; Chen et al., 2009; Hutchinson et al., 2002; Mattay et al., 2002; Naccarato et al., 2006; Riecker et al., 2006; Ward and Frackowiak, 2003). In addition, decreases in functional connectivity and regional homogeneity of low frequency fluctuations at rest have also been reported in the motor network (Wu et al., 2007a; Wu et al., 2007b).

The greatest contribution from any one seed-region came from a region in the left precuneus of the default network (Table 3). The precuneus is thought to be involved in self-referential processing and, as part of the default mode network, is considered a major structural and functional hub of the brain (Cavanna and Trimble, 2006; Hagmann et al., 2008). Age differences in task-related deactivation of the precuneus, and the default network as a whole, have been linked to difficulties in cognitive control that are often apparent in older adults (Grady et al., 2010; Grady et al., 2006; Lustig et al., 2003; Park et al., 2010; Persson et al., 2007; Sambataro et al., 2010). The effects of age on the default network are discussed below.

The differences in correlation coefficients between older adults and younger adults that contributed to the observed feature weights followed three different scenarios (visualized in Figure 3). First, there were those connections that were more positively correlated in older adults than in younger adults. Similar to this, there were those connections that were less negatively correlated in older adults than in younger adults. Finally, there were connections that were less positively correlated in older adults than in younger adults. Each of these scenarios contributed approximately one third of the total summed feature weight used for the SVM classification (Figure 2a). Importantly, connections that strengthened with age, which includes those that increase positive correlation and those that decrease negative correlation, accounted for two thirds of the total weight. This implies that connections that increase in strength with age are the distinguishing characteristics of age-related changes in connectivity, as the SVM classification relied heavily on these connections.

### 4.1. Stronger connections in older adults

A second significant observation from our SVM data presented here is that the connections that were stronger in older adults were mostly between network, or inter-network, connections (Figure 4). This included inter-network connections that became more

positively correlated with age, which were mostly between the sensorimotor network and the two networks previously defined as the task-control networks (the fronto-parietal and cingulo-opercular networks; (Dosenbach et al., 2007; Dosenbach et al., 2006), and also included inter-network connections that became less negatively correlated with age, which were mostly from connections between the default network and the sensorimotor network or the cingulo-opercular network (Figure 4a-b).

The observation that most of the feature weight used to classify older adult brains from younger adult brains came from increasingly positive connections between the sensorimotor network and the task-control networks is consistent with the hypothesis that cognitive systems must compensate in older adults for the general decline in sensorimotor abilities (Li and Lindenberger, 2002; Seidler et al., 2010). For example, Heuninchx et al. have shown that older adults display additional activations not observed in younger adults in cognitive areas including the frontal operculum, dorsolateral PFC, and the superior parietal cortex during simple motor tasks (Heuninckx et al., 2005; Heuninckx et al., 2008). Likewise, an increase in functional connectivity between sensorimotor areas and subcortical regions has been observed during simple motor tasks (Marchand et al., 2011). Our results suggest that the cognitive networks and the sensorimotor networks become less segregated in normal adult aging, possibly due to the greater functional inter-dependence of these networks in older adults. However, it is important to point out that some of the seed-regions classified as sensorimotor by Dosenbach et al. include regions such as the SMA, PMC, and dorsal frontal cortex regions that have previously been implicated in cognitive tasks (Dosenbach et al., 2010).

Another major contribution to our classifier came from connections that had decreases in negative correlations between regions in the default network and regions in the sensorimotor or cingulo-opercular network. It has been documented that the default network is negatively correlated with brain regions that are generally activated during attention-demanding cognitive tasks (Fox et al., 2005; Fransson, 2005). As previously mentioned, older adults often have difficulties in suppressing the default mode network compared to younger adults during cognitive task performance (Grady et al., 2010; Grady et al., 2006; Lustig et al., 2003; Park et al., 2010; Persson et al., 2007; Sambataro et al., 2010). Here, our finding of decreased negative correlations in older adults in connections between the default network and the cingulo-opercular network is consistent with this literature. However, the majority of the feature weight utilized by our classifier that came from decreased negative correlations were from seed-region pairs between the sensorimotor network and default network. It is plausible that this is one consequence of the previously described increased integration of the sensorimotor network and the task-control networks. Further research is needed to investigate the relationship between the default mode network and sensorimotor systems.

### 4.2. Weaker connections in older adults

In contrast to connections that became stronger in older adults, which were mostly internetwork connections, those that became weaker with age were roughly half inter-network and half intra-network, or within network, connections (Figure 4c). Although, as previously noted, much of the feature weight came from seed-regions pairs involving the sensorimotor and cingulo-opercular networks that were more positively correlated in older adults, there were a large number of seed-region pairs involving these networks that became less positively correlated with age. This suggests that the increased involvement of cognition in sensorimotor tasks is a product of substantial reorganization of these two networks, including both increases and decreases in connectivity between the regions.

Our finding that nearly half of the connections that decreased with age were within network connections could reflect the dedifferentiation of these networks with advancing age. This

seems to be the case in particular for the default mode network and the cingulo-opercular network, both of which had lower positive correlations in older adults than younger adults for within network connections (Figure 5). Age-related decreases in functional connectivity within the default network have been documented during task performance and at rest (Andrews-Hanna et al., 2007; Damoiseaux et al., 2008; Grady et al., 2010; Park et al., 2010). Reduced connectivity between areas of the cingulo-opercular network could be linked to difficulties of executive control that are often observed in older adults (for review, see Hedden and Gabrieli, 2004).

## 4.3. Connection distances

In the data presented here there is an age-related weakening of both long-range correlations and negative correlations, and an age-related strengthening of short-range correlations (Figure 6). Thus, the long-range positive and negative correlations that define normal brain organization in healthy adults become less defined in older adults. The reduced connectivity of long range connections observed in our study is in line with a study by Wang et al. that found that there are less long-range connections in older adults than in younger adults during a memory task (Wang et al., 2010). Interestingly, the short-range connections with increasing connectivity with age were mostly between network connections, perhaps reflecting blurring of the functional networks.

## 4.4. Limitations

The present study does have limitations. The use of SVM requires several user decisions, including choosing the number of seed-regions to include and the manner in which seed-regions are defined. We selected seed-regions in an attempt to complement the recent Dosenbach paper that used support vector machines to classify adolescent brains from adult brains (Dosenbach et al., 2010). We also used the same network affiliations of the seed-regions as determined by Dosenbach and colleagues from their community detection analysis. However, the axial slice acquisition of the EPIs prevented the inclusion of the occipital and cerebellar networks in our analysis, as several subjects included in the ICBM dataset did not have coverage in these regions. The use of the entire Dosenbach seed-regions would have been ideal, but the accuracy of our predictor speaks to the robustness of our data. Additionally, although not a limitation, it is important to note that some of the seed-regions in the sensorimotor network have been implicated in cognitive tasks, which might explain the high level of interaction between the sensorimotor and cingulo-opercular networks observed here. It should also be noted that by using Euclidian distance between seed-regions as our measurement for connection length, some of the distances may not truly reflect the structural connective distance, such as for cases in which the measurement was between the hemispheres.

It is possible that factors associated with the scanning sessions themselves contributed to some of the differences observed. However, due to the fact that this dataset was obtained from a data base, detailed information regarding potentially confounding factors such as differences in IQ or the degree to which subjects were able to stay awake during the scans is unfortunately unavailable.

**4.4.1 Group differences in head motion**—One major consideration regarding the current study is that group differences in head movement have been shown by Van Dijk and colleagues to significantly affect correlations between seed-regions (2011). To investigate this issue, a composite score of total motion for each subject was calculated as the square root of the sum of squares of the derivatives for each motion parameter, as suggested by Jones et al (2010). Older adults did have significantly more motion than younger adults ($0.14 \pm 0.013$ in older adults, $0.07 \pm .005$ in younger adults; $t(50) = 4.37$, $p < 0.005$). Motion

parameters were controlled for as nuisance regressors as is standard in the field, although this may not completely control effects introduced by motion as shown by Van Dijk et al (2011). Older subjects had consistently low movement from frame to frame rather than brief periods of large movement precluding frame by frame censoring of the data. We therefore performed three separate analyses to address this issue further (see supplement). First, we performed a second non-linear SVM using a subset of 16 younger subjects and 16 older subjects that were matched in the amount of head motion. This second SVM classified adults at an accuracy of 68%, which is still highly significant ($p < .0005$), and over one third of the consensus features from this analysis were identical to the original analysis (supplementary table 1). Second, we performed a non-linear support vector regression (SVR) on the original 52 subjects with each subjects' composite motion parameter estimate as a dependent variable in order to extract features influenced by their total head motion. From this motion SVR, 76 features were identified of which 27 consensus features overlapped with consensus features derived from the original age SVM (indicated by an asterisk in tables 1 & 2; listed in supplementary table 2). We interpret these 27 features as being sensitive to both age and motion (see a listing of these features as indicated by asterisks in tables 1 & 2; listed in supplementary table 2). We also performed a third analysis of SVM identical to the primary age classifying SVM except without the 76 consensus features derived from the motion SVR. This classifier was 82% accurate, having 99 of its 126 consensus features identical to the original SVM along with 27 additional age-predicting features (see supplement). We interpret these 99 features as a robust set of features sensitive to age-related changes, since the accuracy change was minimal from the original SVM (84% accurate for original age SVM, 82% accurate for the SVM analysis without the 76 motion-influenced features). We also have made note of the 27 additional age-predicting features (supplementary table 3); essentially, the 27 features that overlapped between the motion SVR and the original age SVM were replaced with these 27 additional age-predicting features. However, it must be noted that simply removing the 76 features or connections that were most predictive of head movement does not completely remove the effect that head movement possibly has on the remaining features or connections.

These analyses suggest that motion may account for some of the differences in connectivity observed in this study; however, it is also important to note that for our motion-matched SVM there was a great reduction in power (loss of 10 subjects per group) as a result of matching our groups in terms of head motion. In addition, regression of motion parameters was performed. Although this does not completely eliminate motion-related signal changes, it does reduce the influence of motion. The secondary SVM, and omitting overlapping features based on the motion classifying SVR, are conservative attempts to address the issues of head motion differences in the groups and may result in false negatives. Therefore the paper is mainly focused on all the age-related features, some of which were influenced by motion, and used the entire data set for this study. Certainly, the effect of head motion on functional connectivity analyses needs to be further explored to identify appropriate ways of controlling for group differences that might confound such studies.

### 4.5. Conclusion

These results show that SVM can successfully classify younger adult brains from older adult brains based on their resting-state functional connectivity. More importantly, the use of SVM allowed us to investigate the patterns of age-related connectivity changes that best differentiate older and younger adult brains with confounds typically associated with tasks. We observed three general patterns of resting state functional connectivity that differentiated younger adult brains from older adult brains. The first pattern we observed was that connections between the sensorimotor and cingulo-opercular networks contributed the most to the classifier's accuracy. The second pattern we observed is that there is a decrease in

negative correlations between the default network and the sensorimotor and cingulo-opercular networks. Finally, we observed that within network connections of the cingulo-opercular and default networks were less positively correlated in older adults than in younger adults. These three patterns were observed in the main analysis as well as in the more conservative analyses provided in the supplement in order to account for group differences in head motion (see supplement). Our observation that connections that were more positively correlated in older adults than younger adults were significantly shorter than both connections that were less negatively correlated in older adults and connections that were less positively correlated in older adults was not observed in our more conservative analyses, and it is uncertain whether this finding is due to group differences in head movement or the reduced power of these supplementary analyses.

This study complements the recent study by Dosenbach et al. in which machine learning classifiers were used to predict brain maturity during development (2010). This study also adds to the small body of literature that characterizes age-related reorganization of functional networks with the use of machine learning classifier on resting-state functional connectivity. Better understanding the structural and functional network changes that accompany aging may lead to strategies to ameliorate some of the behavioral consequences of normal aging.

## Supplementary Material

Refer to Web version on PubMed Central for supplementary material.

## Acknowledgments

## References

Andrews-Hanna JR, Snyder AZ, Vincent JL, Lustig C, Head D, Raichle ME, Buckner RL. Disruption of large-scale brain systems in advanced aging. Neuron. 2007; 56:924–935. [PubMed: 18054866]

Biswal B, Yetkin FZ, Haughton VM, Hyde JS. Functional connectivity in the motor cortex of resting human brain using echo-planar MRI. Magn Reson Med. 1995; 34:537–541. [PubMed: 8524021]

Biswal BB, Mennes M, Zuo XN, Gohel S, Kelly C, Smith SM, Beckmann CF, Adelstein JS, Buckner RL, Colcombe S, Dogonowski AM, Ernst M, Fair D, Hampson M, Hoptman MJ, Hyde JS, Kiviniemi VJ, Kotter R, Li SJ, Lin CP, Lowe MJ, Mackay C, Madden DJ, Madsen KH, Margulies DS, Mayberg HS, McMahon K, Monk CS, Mostofsky SH, Nagel BJ, Pekar JJ, Peltier SJ, Petersen SE, Riedl V, Rombouts SA, Rypma B, Schlaggar BL, Schmidt S, Seidler RD, Siegle GJ, Sorg C, Teng GJ, Veijola J, Villringer A, Walter M, Wang L, Weng XC, Whitfield-Gabrieli S, Williamson P, Windischberger C, Zang YF, Zhang HY, Castellanos FX, Milham MP. Toward discovery science of human brain function. Proc Natl Acad Sci U S A. 2010; 107:4734–4739. [PubMed: 20176931]

Calautti C, Serrati C, Baron JC. Effects of age on brain activation during auditory-cued thumb-to-index opposition: A positron emission tomography study. Stroke; a journal of cerebral circulation. 2001; 32:139–146.

Cavanna AE, Trimble MR. The precuneus: a review of its functional anatomy and behavioural correlates. Brain : a journal of neurology. 2006; 129:564–583. [PubMed: 16399806]

Chen NK, Chou YH, Song AW, Madden DJ. Measurement of spontaneous signal fluctuations in fMRI: adult age differences in intrinsic functional connectivity. Brain structure & function. 2009; 213:571–585. [PubMed: 19727810]

Cox RW. AFNI: Software for analysis and visualization of functional magnetic resonance neuroimages. Computers and Biomedical Research. 1996; 29:162–173. [PubMed: 8812068]

Craddock RC, Holtzheimer PE 3rd, Hu XP, Mayberg HS. Disease state prediction from resting state functional connectivity. Magn Reson Med. 2009; 62:1619–1628. [PubMed: 19859933]

Damoiseaux JS, Beckmann CF, Arigita EJ, Barkhof F, Scheltens P, Stam CJ, Smith SM, Rombouts SA. Reduced resting-state brain activity in the "default network" in normal aging. Cereb Cortex. 2008; 18:1856–1864. [PubMed: 18063564]

Dosenbach NU, Fair DA, Miezin FM, Cohen AL, Wenger KK, Dosenbach RA, Fox MD, Snyder AZ, Vincent JL, Raichle ME, Schlaggar BL, Petersen SE. Distinct brain networks for adaptive and stable task control in humans. Proc Natl Acad Sci U S A. 2007; 104:11073–11078. [PubMed: 17576922]

Dosenbach NU, Nardos B, Cohen AL, Fair DA, Power JD, Church JA, Nelson SM, Wig GS, Vogel AC, Lessov-Schlaggar CN, Barnes KA, Dubis JW, Feczko E, Coalson RS, Pruett JR Jr, Barch DM, Petersen SE, Schlaggar BL. Prediction of individual brain maturity using fMRI. Science (New York, N Y). 2010; 329:1358–1361.

Dosenbach NU, Visscher KM, Palmer ED, Miezin FM, Wenger KK, Kang HC, Burgund ED, Grimes AL, Schlaggar BL, Petersen SE. A core system for the implementation of task sets. Neuron. 2006; 50:799–812. [PubMed: 16731517]

Fox MD, Snyder AZ, Vincent JL, Corbetta M, Van Essen DC, Raichle ME. The human brain is intrinsically organized into dynamic, anticorrelated functional networks. Proc Natl Acad Sci U S A. 2005; 102:9673–9678. [PubMed: 15976020]

Fransson P. Spontaneous low-frequency BOLD signal fluctuations: an fMRI investigation of the resting-state default mode of brain function hypothesis. Hum Brain Mapp. 2005; 26:15–29. [PubMed: 15852468]

Grady CL, Protzner AB, Kovacevic N, Strother SC, Afshin-Pour B, Wojtowicz M, Anderson JA, Churchill N, McIntosh AR. A multivariate analysis of age-related differences in default mode and task-positive networks across multiple cognitive domains. Cereb Cortex. 2010; 20:1432–1447. [PubMed: 19789183]

Grady CL, Springer MV, Hongwanishkul D, McIntosh AR, Winocur G. Age-related changes in brain activity across the adult lifespan. Journal of cognitive neuroscience. 2006; 18:227–241. [PubMed: 16494683]

Hagmann P, Cammoun L, Gigandet X, Meuli R, Honey CJ, Wedeen VJ, Sporns O. Mapping the structural core of human cerebral cortex. PLoS biology. 2008; 6:e159. [PubMed: 18597554]

Hedden T, Gabrieli JD. Insights into the ageing mind: a view from cognitive neuroscience. Nat Rev Neurosci. 2004; 5:87–96. [PubMed: 14735112]

Heuninckx S, Wenderoth N, Debaere F, Peeters R, Swinnen SP. Neural basis of aging: the penetration of cognition into action control. J Neurosci. 2005; 25:6787–6796. [PubMed: 16033888]

Heuninckx S, Wenderoth N, Swinnen SP. Systems neuroplasticity in the aging brain: recruiting additional neural resources for successful motor performance in elderly persons. J Neurosci. 2008; 28:91–99. [PubMed: 18171926]

Hutchinson S, Kobayashi M, Horkan CM, Pascual-Leone A, Alexander MP, Schlaug G. Age-related differences in movement representation. Neuroimage. 2002; 17:1720–1728. [PubMed: 12498746]

Jones TB, Bandettini PA, Kenworthy L, Case LK, Milleville SC, Martin A, Birn RM. Sources of group differences in functional connectivity: an investigation applied to autism spectrum disorder. Neuroimage. 2010; 49:401–414. [PubMed: 19646533]

Li KZ, Lindenberger U. Relations between aging sensory/sensorimotor and cognitive functions. Neurosci Biobehav Rev. 2002; 26:777–783. [PubMed: 12470689]

Lustig C, Snyder AZ, Bhakta M, O'Brien KC, McAvoy M, Raichle ME, Morris JC, Buckner RL. Functional deactivations: change with age and dementia of the Alzheimer type. Proceedings of the National Academy of Sciences of the United States of America. 2003; 100:14504–14509. [PubMed: 14608034]

Marchand WR, Lee JN, Suchy Y, Garn C, Johnson S, Wood N, Chelune G. Age-related changes of the functional architecture of the cortico-basal ganglia circuitry during motor task execution. Neuroimage. 2011; 55:194–203. [PubMed: 21167945]

Mattay VS, Fera F, Tessitore A, Hariri AR, Das S, Callicott JH, Weinberger DR. Neurophysiological correlates of age-related changes in human motor function. Neurology. 2002; 58:630–635. [PubMed: 11865144]

Meunier D, Achard S, Morcom A, Bullmore E. Age-related changes in modular organization of human brain functional networks. Neuroimage. 2009; 44:715–723. [PubMed: 19027073]

Naccarato M, Calautti C, Jones PS, Day DJ, Carpenter TA, Baron JC. Does healthy aging affect the hemispheric activation balance during paced index-to-thumb opposition task? An fMRI study. Neuroimage. 2006; 32:1250–1256. [PubMed: 16806984]

Park DC, Polk TA, Hebrank AC, Jenkins LJ. Age differences in default mode activity on easy and difficult spatial judgment tasks. Frontiers in human neuroscience. 2010; 3:75. [PubMed: 20126437]

Pereira F, Mitchell T, Botvinick M. Machine learning classifiers and fMRI: a tutorial overview. Neuroimage. 2009; 45:S199–209. [PubMed: 19070668]

Persson J, Lustig C, Nelson JK, Reuter-Lorenz PA. Age differences in deactivation: a link to cognitive control? Journal of cognitive neuroscience. 2007; 19:1021–1032. [PubMed: 17536972]

Riecker A, Groschel K, Ackermann H, Steinbrink C, Witte O, Kastrup A. Functional significance of age-related differences in motor activation patterns. Neuroimage. 2006; 32:1345–1354. [PubMed: 16798017]

Sambataro F, Murty VP, Callicott JH, Tan HY, Das S, Weinberger DR, Mattay VS. Age-related alterations in default mode network: impact on working memory performance. Neurobiol Aging. 2010; 31:839–852. [PubMed: 18674847]

Scholkopf B, Mika S, Burges CC, Knirsch P, Muller KR, Ratsch G, Smola AJ. Input space versus feature space in kernel-based methods. IEEE Trans Neural Netw. 1999; 10:1000–1017. [PubMed: 18252603]

Seidler RD, Bernard JA, Burutolu TB, Fling BW, Gordon MT, Gwin JT, Kwak Y, Lipps DB. Motor control and aging: links to age-related brain structural, functional, and biochemical effects. Neurosci Biobehav Rev. 2010; 34:721–733. [PubMed: 19850077]

Shen H, Wang L, Liu Y, Hu D. Discriminative analysis of resting-state functional connectivity patterns of schizophrenia using low dimensional embedding of fMRI. Neuroimage. 2010; 49:3110–3121. [PubMed: 19931396]

Smith SM, Fox PT, Miller KL, Glahn DC, Fox PM, Mackay CE, Filippini N, Watkins KE, Toro R, Laird AR, Beckmann CF. Correspondence of the brain's functional architecture during activation and rest. Proc Natl Acad Sci U S A. 2009; 106:13040–13045. [PubMed: 19620724]

Smith SM, Jenkinson M, Woolrich MW, Beckmann CF, Behrens TEJ, Johansen-Berg H, Bannister PR, DeLuca M, Drobnjak I, Flitney DE, Niazy R, Saunders J, Vickers J, Zhang Y, De Stefano N, Brady JM, Matthews PM. Advances in functional and structural MR image analysis and implementation as FSL. Neuroimage. 2004; 23:208–219.

Supekar K, Musen M, Menon V. Development of large-scale functional brain networks in children. PLoS Biol. 2009; 7:e1000157. [PubMed: 19621066]

Van Dijk KR, Sabuncu MR, Buckner RL. The influence of head motion on intrinsic functional connectivity MRI. Neuroimage. 2011

Wang L, Li Y, Metzak P, He Y, Woodward TS. Age-related changes in topological patterns of large-scale brain functional networks during memory encoding and recognition. Neuroimage. 2010; 50:862–872. [PubMed: 20093190]

Ward NS, Frackowiak RS. Age-related changes in the neural correlates of motor performance. Brain : a journal of neurology. 2003; 126:873–888. [PubMed: 12615645]

Weston J, Elisseeff A, Baklr G, Sinz F. The Spider Machine Learning Toolbox. 2005

Woolrich MW, Jbabdi S, Patenaude B, Chappell M, Makni S, Behrens T, Beckmann C, Jenkinson M, Smith SM. Bayesian analysis of neuroimaging data in FSL. Neuroimage. 2009; 45:173–186.

Wu T, Zang Y, Wang L, Long X, Hallett M, Chen Y, Li K, Chan P. Aging influence on functional connectivity of the motor network in the resting state. Neuroscience letters. 2007a; 422:164–168. [PubMed: 17611031]

Wu T, Zang Y, Wang L, Long X, Li K, Chan P. Normal aging decreases regional homogeneity of the motor areas in the resting state. Neuroscience letters. 2007b; 423:189–193. [PubMed: 17709202]

Zuo XN, Kelly C, Di Martino A, Mennes M, Margulies DS, Bangaru S, Grzadzinski R, Evans AC, Zang YF, Castellanos FX, Milham MP. Growing together and growing apart: regional and sex differences in the lifespan developmental trajectories of functional homotopy. J Neurosci. 2010; 30:15034–15043. [PubMed: 21068309]
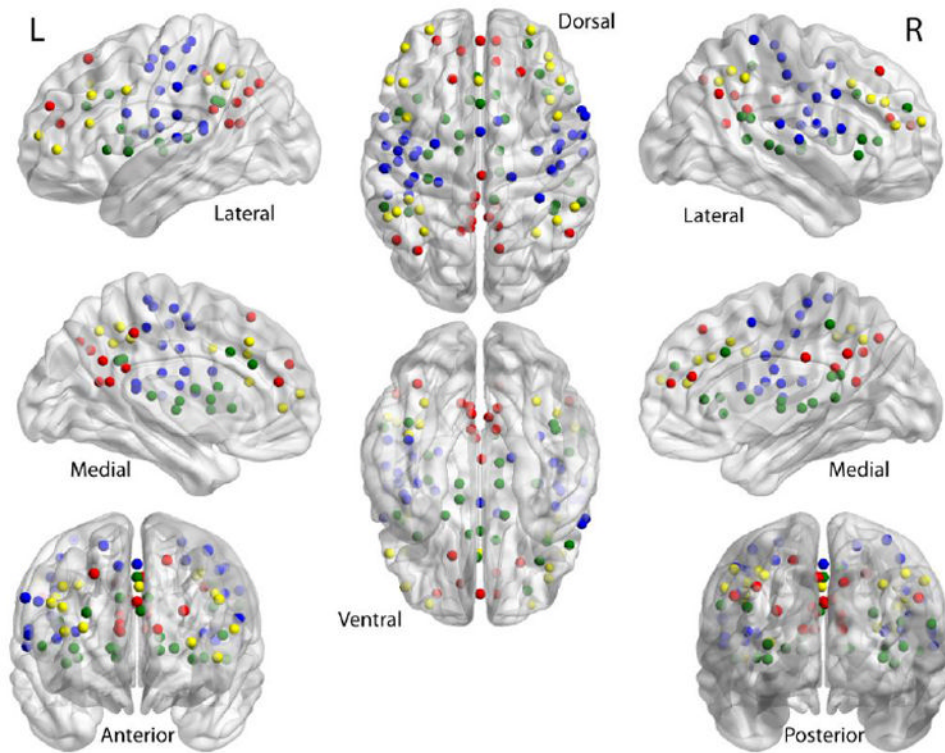
**Figure 1.**
Shown are the 100 seed-regions used in this study taken from Dosenbach et al. (2010).
Fronto-parietal network is in yellow; sensorimotor in blue; default in red; cingulo-opercular in green.
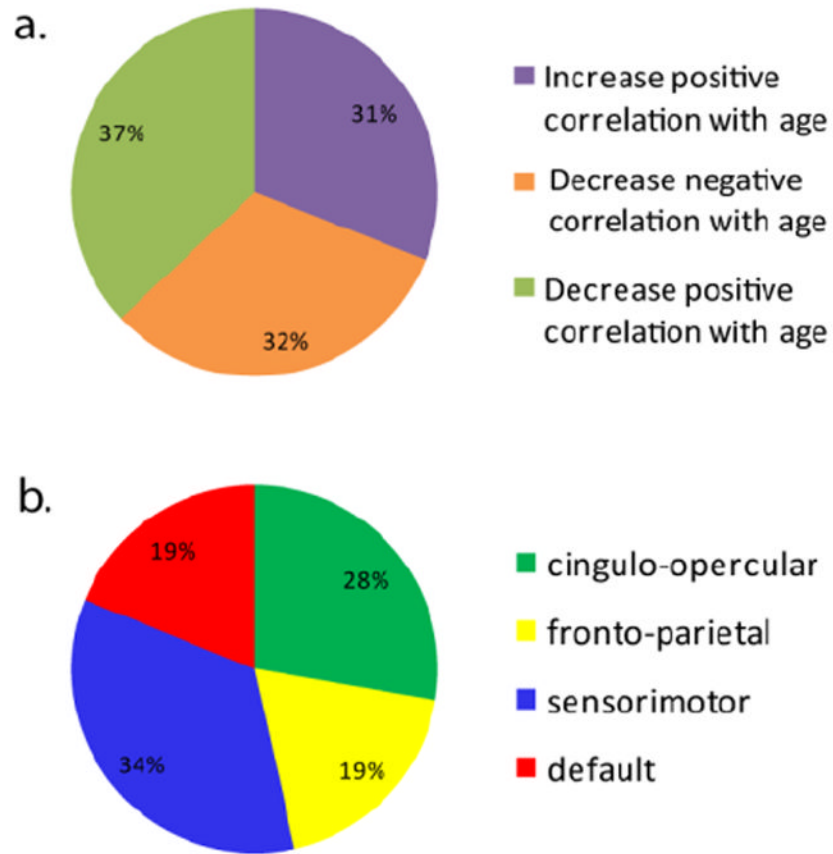
**Figure 2.**
Pie charts illustrating the percentage of the total weight that came from each (*a*) scenario observed and (*b*) network studied.
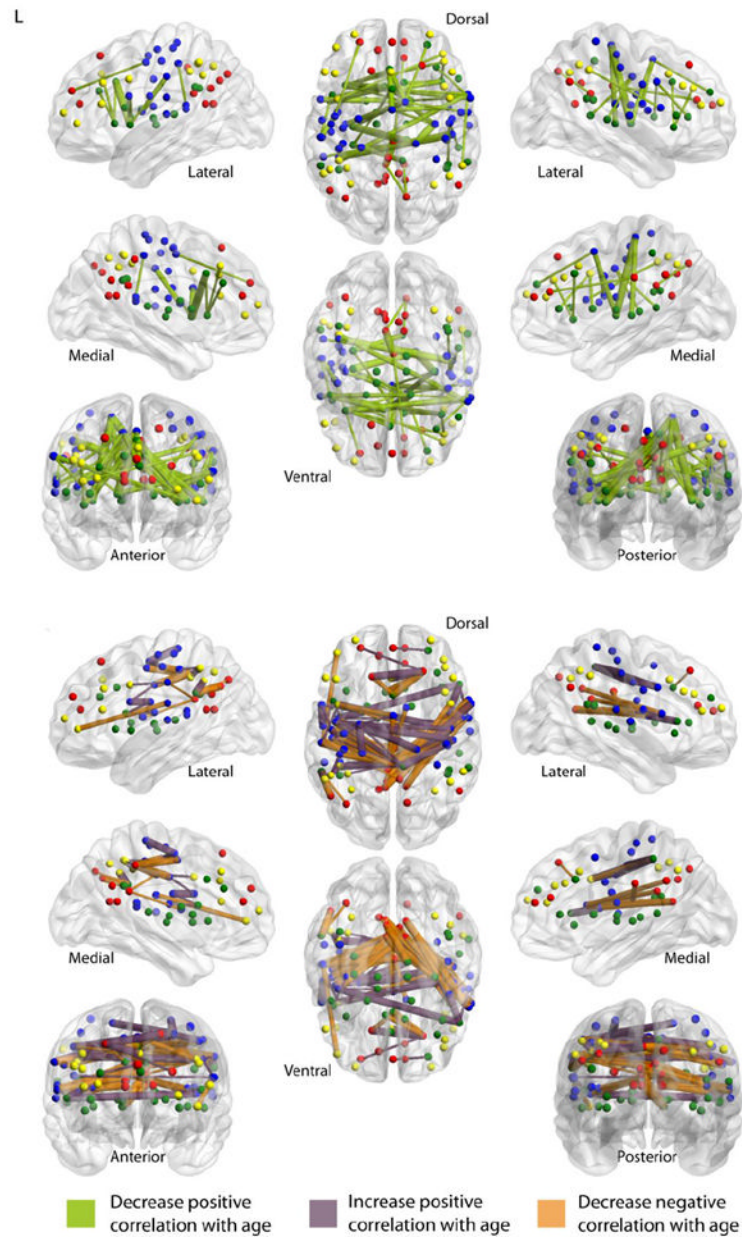
**Figure 3.**
Illustration of the consensus features that decreased positive correlation with age (top) and the consensus features that increased positive correlation with age and decreased negative correlation with age (bottom). Connections are scaled by their respective feature weight, with thicker connections representing greater feature weight.
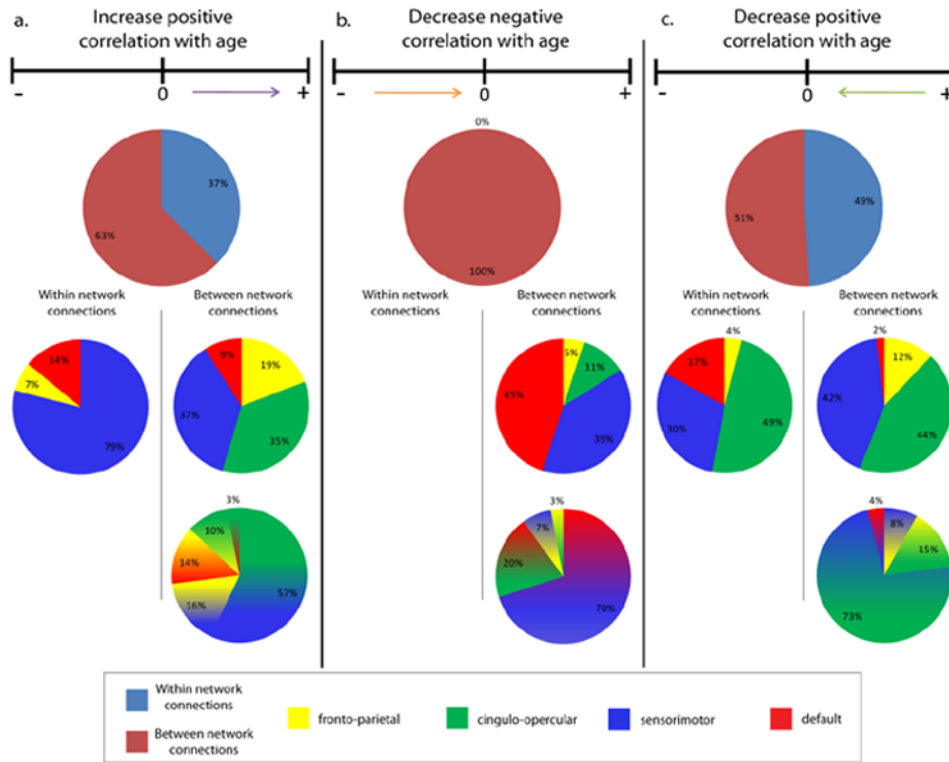
**Figure 4.**
Pie charts illustrating the breakdown of the feature weight coming from (*a*) connections that are more positively correlated with age, (*b*) connections that are less negatively correlated with age, and (*c*) connections that are less positively correlated with age as being between network or within network, and the breakdown of these connection types based on the contributing network or networks.
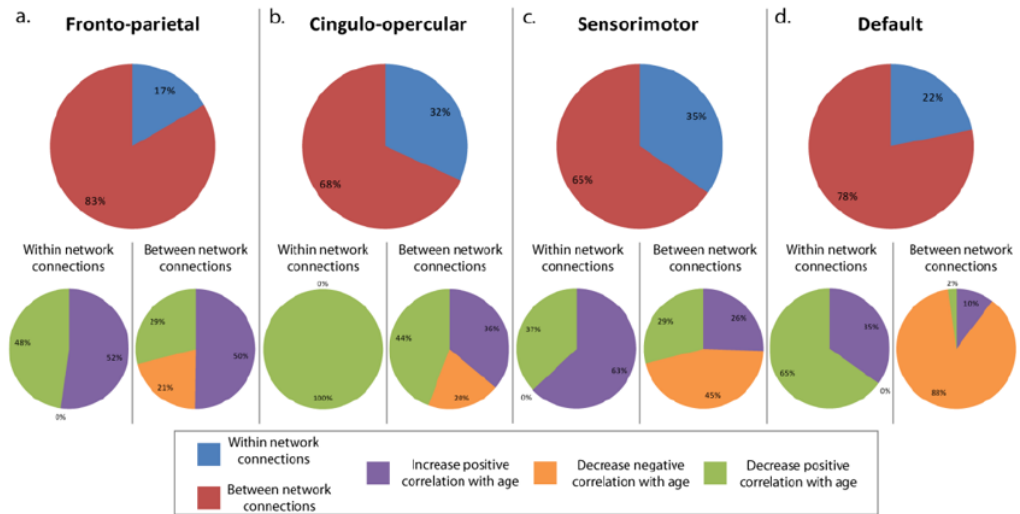
**Figure 5.**
Pie charts illustrating the percentage of feature weight coming from between network connections and within network connections for the (a) fronto-parietal network, (b) cingulo-opercular network, (c) sensorimotor network, and (d) the default network. Shows the percentage of the feature weight coming from within and between network connections that either increased positive correlation with age, decreased negative correlation with age, or decreased positive correlation with age is also shown for each network.
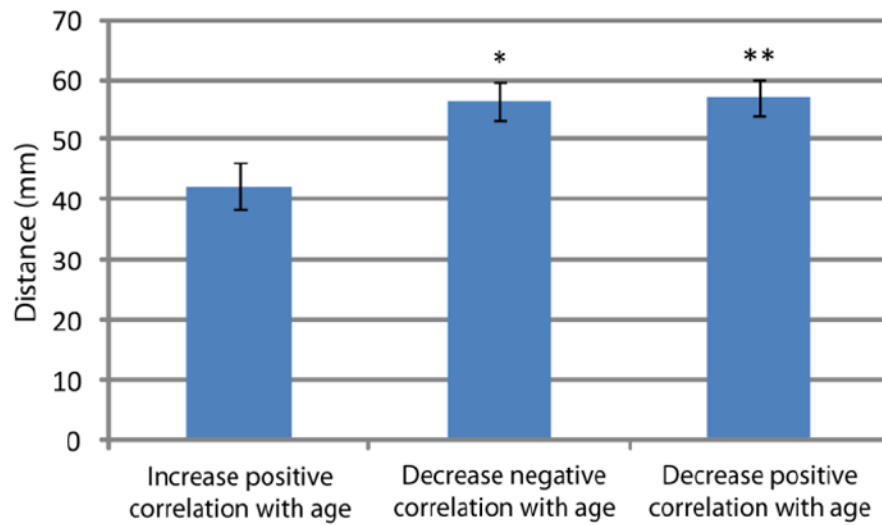
**Figure 6.**
Connections that were more positively correlated in older adults than younger adults were significantly shorter than both connections that were less negatively correlated in older adults (t(76) = -2.826, * p < 0.01)) and connections that were less positively correlated in older adults (t(84) = -3.112, **p < 0.005)). Based on Euclidian distance. Error bars are the standard error of the mean.

**Table 1**

Information on consensus features with negative feature weights derived from connections that were more positively correlated (or less negatively correlated) in older adults than in younger adults. Shown are the seed-region pairs and their respective networks, the average feature weight for each seed-region pair, and the respective z-transformed correlation coefficients for both the younger and older adult groups.

| | Network 1 | Seed 1 | Consensus Features | | | Weight | zCC | |
| | | | Network 2 | Seed 2 | | | Young | Old |
|---|---|---|---|---|---|---|---|---|
| * | fronto-parietal | L_IPL_1 | default | L_precuneus_1 | | -6.9637 | 0.026 | 0.324 |
| * | sensorimotor | L_parietal_1 | sensorimotor | R_parietal_3 | | -6.8139 | 0.14344 | 0.41574 |
| | cingulo-opercular | L_parietal_8 | fronto-parietal | L_IPL_3 | | -6.4236 | 0.4054 | 0.71477 |
| * | sensorimotor | L_parietal_5 | default | L_precuneus_1 | | -6.3416 | -0.07283 | 0.19833 |
| * | cingulo-opercular | M_mFC | default | R_sup_frontal | | -6.0915 | -0.07322 | 0.19149 |
| * | sensorimotor | R_parietal_1 | default | L_precuneus_1 | | -6.037 | -0.06051 | 0.23221 |
| * | sensorimotor | L_vFC_2 | sensorimotor | L_precentral_gyrus_2 | | -5.9828 | 0.27595 | 0.49152 |
| | cingulo-opercular | R_precuneus_1 | sensorimotor | R_dFC_3 | | -5.9076 | 0.00677 | 0.20285 |
| * | cingulo-opercular | R_basal_ganglia_2 | default | L_post_cingulate_1 | | -5.8994 | -0.04513 | 0.15182 |
| | sensorimotor | L_parietal_2 | default | L_precuneus_1 | | -5.8611 | -0.08508 | 0.1419 |
| * | cingulo-opercular | R_vFC_1 | sensorimotor | L_mid_insula_1 | | -5.8045 | 0.05756 | 0.28137 |
| | default | L_sup_frontal | default | R_sup_frontal | | -5.785 | 0.31145 | 0.53908 |
| * | sensorimotor | L_parietal_4 | default | L_precuneus_1 | | -5.7482 | -0.07106 | 0.18429 |
| | cingulo-opercular | R_vFC_1 | sensorimotor | R_vFC_2 | | -5.6727 | 0.10371 | 0.32266 |
| * | fronto-parietal | M_ACC_2 | default | R_sup_frontal | | -5.5557 | 0.12497 | 0.36098 |
| | sensorimotor | R_frontal_2 | default | L_precuneus_1 | | -5.5424 | -0.13916 | 0.09649 |
| | cingulo-opercular | R_basal_ganglia_2 | default | L_post_cingulate_2 | | -5.5077 | -0.00997 | 0.19253 |
| * | sensorimotor | L_parietal_1 | sensorimotor | R_parietal_1 | | -5.443 | 0.11674 | 0.31418 |
| | sensorimotor | L_parietal_1 | sensorimotor | L_parietal_7 | | -5.4388 | 0.12552 | 0.38364 |
| | sensorimotor | R_frontal_1 | default | R_post_cingulate | | -5.4126 | -0.33475 | -0.09609 |
| | sensorimotor | L_precentral_gyrus_1 | default | L_precuneus_1 | | -5.3767 | -0.09455 | 0.13864 |
| | cingulo-opercular | R_precuneus_1 | sensorimotor | R_precentral_gyrus_3 | | -5.3665 | 0.09811 | 0.29391 |
| * | cingulo-opercular | R_precuneus_1 | sensorimotor | R_parietal_1 | | -5.3601 | 0.13225 | 0.34745 |
| | cingulo-opercular | L_parietal_8 | default | L_angular_gyrus_2 | | -5.3436 | -0.02154 | 0.26414 |
| * | sensorimotor | R_precentral_gyrus_3 | default | L_precuneus_1 | | -5.3309 | -0.05766 | 0.1785 |
| * | sensorimotor | R_frontal_1 | default | L_precuneus_2 | | -5.3051 | -0.40751 | -0.17159 |

|  | Consensus Features |  |  |  | Weight | zCC | |
|---|---|---|---|---|---|---|---|
|  | Network 1 | Seed 1 | Network 2 | Seed 2 | | Young | Old |
| * | sensorimotor | R_dFC_3 | default | L_precuneus_1 | -5.3008 | -0.13199 | 0.08819 |
| | fronto-parietal | L_dFC | sensorimotor | R_precentral_gyrus_3 | -5.215 | 0.0284 | 0.20884 |
| | sensorimotor | L_parietal_5 | default | M_post_cingulate | -5.214 | -0.186 | 0.00616 |
| * | sensorimotor | R_frontal_1 | default | R_precuneus_3 | -5.1548 | -0.38606 | -0.17114 |
| | sensorimotor | L_parietal_1 | sensorimotor | R_precentral_gyrus_3 | -5.0597 | 0.00014 | 0.17029 |
| | sensorimotor | R_pre_SMA | default | L_precuneus_1 | -5.0595 | -0.01934 | 0.182 |
| * | cingulo-opercular | R_precuneus_1 | sensorimotor | L_precentral_gyrus_1 | -5.0434 | 0.03514 | 0.22223 |
| | sensorimotor | R_frontal_1 | default | L_post_cingulate_1 | -5.0271 | -0.2892 | -0.06083 |
| | sensorimotor | L_mid_insula_1 | default | R_precuneus_2 | -4.9988 | -0.11259 | 0.08349 |
| * | cingulo-opercular | R_precuneus_1 | fronto-parietal | R_dFC_2 | -4.9833 | -0.02671 | 0.15223 |
| * | sensorimotor | L_post_parietal_1 | default | L_precuneus_1 | -4.9758 | -0.00006 | 0.22795 |
| | sensorimotor | M_SMA | default | L_precuneus_1 | -4.9607 | -0.02843 | 0.19909 |
| | sensorimotor | R_post_insula | default | M_post_cingulate | -4.9419 | -0.09243 | 0.09829 |
| | fronto-parietal | L_parietal_1 | sensorimotor | L_parietal_4 | -4.9403 | 0.2186 | 0.43343 |
| | sensorimotor | L_vent_aPFC | sensorimotor | L_precentral_gyrus_3 | -4.938 | -0.08357 | 0.07917 |
| | sensorimotor | L_precentral_gyrus_1 | sensorimotor | L_parietal_1 | -4.8991 | 0.24984 | 0.44281 |
| | fronto-parietal | R_vFC_2 | default | R_post_cingulate | -4.8767 | -0.15563 | 0.02577 |
| | fronto-parietal | L_dFC | sensorimotor | M_SMA | -4.8728 | -0.03186 | 0.13673 |
| * | fronto-parietal | L_IPL_1 | fronto-parietal | L_IPL_2 | -4.8506 | 0.39204 | 0.59056 |
| | cingulo-opercular | L_basal_ganglia_1 | default | R_sup_frontal | -4.8298 | -0.15502 | 0.02432 |
| | fronto-parietal | R_dFC_2 | sensorimotor | R_precentral_gyrus_3 | -4.7777 | 0.07521 | 0.26542 |
| * | sensorimotor | R_frontal_1 | default | R_precuneus_2 | -4.7749 | -0.22408 | -0.0175 |
| | cingulo-opercular | M_mFC | default | L_sup_frontal | -4.7542 | -0.08898 | 0.10304 |
| | sensorimotor | L_mid_insula_2 | default | R_precuneus_2 | -4.7339 | -0.04408 | 0.14061 |
| * | sensorimotor | L_precentral_gyrus_1 | sensorimotor | R_parietal_3 | -4.6947 | 0.12362 | 0.30584 |
| * | cingulo-opercular | R_vFC_1 | sensorimotor | R_mid_insula_1 | -4.6941 | 0.06274 | 0.22645 |
| * | sensorimotor | R_frontal_1 | default | L_post_cingulate_3 | -4.6882 | -0.35517 | -0.14138 |
| * | cingulo-opercular | R_aPFC_2 | default | M_mPFC | -4.6811 | 0.11098 | 0.34963 |
| | sensorimotor | L_vFC_2 | sensorimotor | R_precentral_gyrus_2 | -4.6715 | 0.20328 | 0.36102 |
| | sensorimotor | L_vFC_2 | sensorimotor | L_parietal_2 | -4.6594 | 0.1762 | 0.35079 |

| | Consensus Features | | | | Weight | zCC | |
|---|---|---|---|---|---|---|---|
| | Network 1 | Seed 1 | Network 2 | Seed 2 | | Young | Old |
| | fronto-parietal | L_dFC | sensorimotor | L_parietal_5 | -4.5916 | 0.02255 | 0.19673 |
| * | cingulo-opercular | L_vFC_1 | sensorimotor | L_precentral_gyrus_2 | -4.5639 | 0.1151 | 0.26631 |
| | cingulo-opercular | L_thalamus_1 | sensorimotor | L_mid_insula_1 | -4.5524 | 0.13101 | 0.34489 |
| | cingulo-opercular | R_precuneus_1 | sensorimotor | L_parietal_1 | -4.541 | 0.10812 | 0.2848 |
| | sensorimotor | L_parietal_1 | sensorimotor | M_SMA | -4.5282 | 0.4107 | 0.59782 |
| | cingulo-opercular | R_precuneus_1 | fronto-parietal | L_IPL_1 | -4.5181 | 0.08958 | 0.24964 |
| | fronto-parietal | L_dFC | sensorimotor | R_parietal_1 | -4.5076 | -0.0236 | 0.1464 |
| | sensorimotor | L_mid_insula_1 | default | L_post_cingulate_1 | -4.4725 | -0.1563 | 0.02463 |
| | cingulo-opercular | R_precuneus_1 | sensorimotor | L_parietal_4 | -4.4683 | 0.1485 | 0.31761 |
| | cingulo-opercular | L_parietal_8 | default | L_IPS_2 | -4.4477 | -0.13155 | 0.07914 |
| | sensorimotor | L_parietal_5 | default | L_post_cingulate_1 | -4.4456 | -0.22846 | -0.08524 |
| | sensorimotor | R_precentral_gyrus_1 | default | R_post_cingulate | -4.4272 | -0.1245 | 0.03998 |
| | sensorimotor | L_parietal_2 | default | M_post_cingulate | -4.4161 | -0.16392 | 0.00723 |
| | sensorimotor | L_parietal_5 | default | R_precuneus_3 | -4.4074 | -0.1752 | -0.01556 |
| * | fronto-parietal | L_IPL_2 | sensorimotor | L_post_parietal_1 | -4.3931 | 0.03602 | 0.23119 |
| | cingulo-opercular | R_precuneus_1 | sensorimotor | L_parietal_2 | -4.3759 | 0.0748 | 0.23352 |
| | default | L_aPFC_2 | default | R_sup_frontal | -4.3651 | 0.00635 | 0.19928 |
| * | fronto-parietal | L_post_parietal_2 | default | L_precuneus_1 | -4.3286 | 0.06226 | 0.2472 |
| * | sensorimotor | R_precentral_gyrus_1 | default | R_precuneus_2 | -4.3278 | -0.16687 | -0.00511 |
| | cingulo-opercular | L_vFC_1 | sensorimotor | L_mid_insula_2 | -4.3116 | 0.14899 | 0.30957 |
| | cingulo-opercular | R_dACC | default | R_sup_frontal | -4.2573 | -0.10625 | 0.05787 |
| | cingulo-opercular | R_vFC_1 | sensorimotor | R_precentral_gyrus_1 | -4.2376 | 0.01835 | 0.18367 |

Features that overlap with features derived from the motion-SVR (see supplement) indicated with *. ROI seeds are coded for ease of visualization in Tables 1-3: fronto-parietal – yellow; sensorimotor – blue; default – red; cingulo-opercular – green.

**Table 2**

Information on consensus features with positive feature weights derived from connections that were more positively correlated in younger adults than in older adults. Shown are the seed-region pairs and their respective networks, the average feature weights for each seed-region pair, and the respective z-transformed correlation coefficients for both the younger and older adult groups.

| Consensus Features | | | | Weight | zCC | |
|---|---|---|---|---|---|---|
| Network 1 | Seed 1 | Network 2 | Seed 2 | | Young | Old |
| cingulo-opercular | L_ant_insula | cingulo-opercular | M_mFC | 7.0028 | 0.416 | 0.166 |
| cingulo-opercular | R_mid_insula_2 | sensorimotor | R_parietal_3 | 6.2496 | 0.13351 | -0.06179 |
| cingulo-opercular | R_basal_ganglia_1 | cingulo-opercular | M_mFC | 5.74 | 0.23981 | 0.05116 |
| sensorimotor | L_temporal_2 | sensorimotor | R_parietal_1 | 5.4257 | 0.16448 | -0.03993 |
| cingulo-opercular | L_mid_insula_3 | sensorimotor | R_parietal_3 | 5.3 | 0.07934 | -0.09357 |
| default | L_post_cingulate_1 | default | M_post_cingulate | 5.2879 | 0.71585 | 0.50237 |
| cingulo-opercular | L_vFC_3 | cingulo-opercular | L_basal_ganglia_1 | 5.1761 | 0.31143 | 0.11882 |
| sensorimotor | L_mid_insula_1 | sensorimotor | L_parietal_5 | 5.1124 | 0.27156 | 0.06977 |
| cingulo-opercular | L_post_insula | cingulo-opercular | R_precuneus_1 | 5.1106 | 0.05066 | -0.09328 |
| cingulo-opercular | M_ACC_1 | sensorimotor | M_SMA | 4.977 | 0.09544 | -0.07402 |
| cingulo-opercular | M_ACC_1 | sensorimotor | R_pre_SMA | 4.9165 | 0.15591 | -0.0049 |
| sensorimotor | R_vFC_2 | sensorimotor | M_SMA | 4.9102 | 0.29728 | 0.10816 |
| cingulo-opercular | R_basal_ganglia_1 | sensorimotor | L_vFC_2 | 4.9018 | 0.065 | -0.10551 |
| cingulo-opercular | L_ant_insula | sensorimotor | R_dFC_3 | 4.8627 | 0.12801 | -0.06275 |
| cingulo-opercular | R_mid_insula_2 | sensorimotor | R_pre_SMA | 4.7979 | 0.16215 | 0.01979 |
| cingulo-opercular | L_basal_ganglia_2 | sensorimotor | L_vFC_2 | 4.7975 | 0.13288 | -0.01373 |
| cingulo-opercular | R_ant_insula | cingulo-opercular | M_mFC | 4.7868 | 0.36379 | 0.19215 |
| fronto-parietal | L_IPL_1 | sensorimotor | R_frontal_1 | 4.7661 | 0.24419 | 0.04502 |
| sensorimotor | L_mid_insula_2 | sensorimotor | R_pre_SMA | 4.7616 | 0.11863 | -0.01357 |
| cingulo-opercular | R_basal_ganglia_2 | sensorimotor | R_parietal_3 | 4.7302 | 0.09986 | -0.05815 |
| cingulo-opercular | L_ant_insula | cingulo-opercular | L_basal_ganglia_1 | 4.6473 | 0.34985 | 0.16561 |
| sensorimotor | L_precentral_gyrus_1 | default | L_aPFC_2 | 4.6358 | 0.0399 | -0.12346 |
| default | R_ACC | default | M_post_cingulate | 4.6356 | 0.34947 | 0.1559 |
| cingulo-opercular | L_thalamus_1 | cingulo-opercular | M_mFC | 4.6113 | 0.13332 | -0.01663 |
| cingulo-opercular | L_ant_insula | fronto-parietal | M_ACC_2 | 4.6103 | 0.27293 | 0.10616 |
| cingulo-opercular | R_aPFC_2 | sensorimotor | R_pre_SMA | 4.5785 | 0.16879 | 0.00282 |

*

| | Consensus Features | | | Weight | zCC | |
| --- | --- | --- | --- | --- | --- | --- |
| Network 1 | Seed 1 | Network 2 | Seed 2 | | Young | Old |
| cingulo-opercular | L_mid_insula_3 | sensorimotor | R_pre_SMA | 4.5591 | 0.09643 | -0.03078 |
| sensorimotor | L_temporal_3 | sensorimotor | R_parietal_1 | 4.5587 | 0.15899 | -0.0075 |
| cingulo-opercular | R_mid_insula_2 | sensorimotor | M_SMA | 4.5469 | 0.14311 | -0.01256 |
| default | L_post_cingulate_1 | default | R_precuneus_4 | 4.5457 | 0.26562 | 0.0622 |
| cingulo-opercular | L_ant_insula | cingulo-opercular | M_ACC_1 | 4.5381 | 0.28149 | 0.10303 |
| default | R_precuneus_2 | default | R_precuneus_4 | 4.5077 | 0.30916 | 0.1291 |
| cingulo-opercular | M_mFC | sensorimotor | R_frontal_1 | 4.5062 | 0.24623 | 0.0819 |
| sensorimotor | L_post_parietal_1 | sensorimotor | L_temporal_2 | 4.4753 | 0.14963 | -0.02755 |
| cingulo-opercular | L_vFC_3 | sensorimotor | L_parietal_5 | 4.4663 | 0.10568 | -0.05657 |
| cingulo-opercular | R_temporal_2 | sensorimotor | R_precentral_gyrus_3 | 4.4644 | 0.15667 | 0.00187 |
| fronto-parietal | L_dFC | fronto-parietal | R_vlPFC | 4.4437 | 0.10913 | -0.06178 |
| cingulo-opercular | R_ant_insula | fronto-parietal | R_dlPFC_1 | 4.4428 | 0.4023 | 0.1982 |
| cingulo-opercular | R_temporal_3 | sensorimotor | R_precentral_gyrus_3 | 4.4342 | 0.0595 | -0.08722 |
| sensorimotor | R_pre_SMA | sensorimotor | R_precentral_gyrus_1 | 4.4261 | 0.14524 | 0.01156 |
| fronto-parietal | R_IPL_1 | sensorimotor | R_frontal_1 | 4.4176 | 0.31142 | 0.10737 |
| cingulo-opercular | L_ant_insula | fronto-parietal | R_dlPFC_1 | 4.4089 | 0.32468 | 0.13562 |
| cingulo-opercular | R_basal_ganglia_1 | fronto-parietal | R_dFC_2 | 4.408 | 0.10857 | -0.04004 |
| cingulo-opercular | L_vFC_3 | cingulo-opercular | M_mFC | 4.3863 | 0.25435 | 0.10965 |
| cingulo-opercular | R_vPFC | sensorimotor | R_dFC_3 | 4.3446 | 0.09467 | -0.04865 |
| cingulo-opercular | L_post_insula | cingulo-opercular | M_mFC | 4.3383 | 0.02779 | -0.10139 |
| cingulo-opercular | L_ant_insula | sensorimotor | R_pre_SMA | 4.3322 | 0.28154 | 0.11907 |
| cingulo-opercular | R_ant_insula | cingulo-opercular | R_dACC | 4.323 | 0.35691 | 0.19289 |

Features that overlap with features derived from the motion-SVR (see supplement) indicated with *.

**Table 3**

Listed are the top 10 seed-regions with their MNI coordinates and their respective networks ranked by the sum of 1/2 of all the feature weight coming from connections involving that seed-region.

| Network | Seed | X | Y | Z |
|---|---|---|---|---|
| default | L_precuneus_1 | -3 | -38 | 45 |
| sensorimotor | R_parietal_1 | 46 | -20 | 45 |
| sensorimotor | R_pre_SMA | 10 | 5 | 51 |
| sensorimotor | M_SMA | 0 | -1 | 52 |
| cingulo-opercular | R_precuneus_1 | 8 | -40 | 50 |
| cingulo-opercular | M_mFC | 0 | 15 | 45 |
| sensorimotor | R_frontal_1 | 58 | 11 | 14 |
| sensorimotor | L_parietal_5 | -55 | -22 | 38 |
| fronto-parietal | L_dFC | -42 | 7 | 36 |
| cingulo-opercular | L_ant_insula | -36 | 18 | 2 |